Chin. J. Astron. Astrophys. Vol. 6 (2006), No. 2, 125–140
(*http://www.chjaa.org*)

Chinese Journal of
Astronomy and
Astrophysics

On the Calculation of Lyapunov Indicators with Post-stabilization in a Weyl Field *

Xin Wu[1,2], Hong Zhang[2] and Xiao-Sheng Wan[2]

[1] Department of Physics, Nanchang University, Nanchang 330047; *xwu@ncu.edu.cn*
[2] Department of Astronomy, Nanjing University, Nanjing 210093; *xinwu@nju.edu.cn*

Received 2005 August 24; accepted 2005 December 4

Abstract We present details of a work aiming at the overestimation of Lyapunov exponents defined by the geodesic deviation equations in the previous work. The geodesic deviation vector with post-stabilization is used to compute the fast Lyapunov indicator, considered to be a very sensitive tool for discrimination between ordered or weakly chaotic motions. We make a detailed study of the dynamics in the superposed Weyl field between a black hole and shell of octopoles by using the fast Lyapunov indicator with the Poincaré surface of section. In particular, we examine the effects on the dynamics around the fixed points, of varying one of the three parameters (specific energy E, specific angular momentum L and octopolar moment $\mathcal{O}$), while keeping the other two fixed, and identify the intervals of the varying parameter where the motion is regular or chaotic.

Key words: black hole physics — stars: circumstellar matter — chaos — methods: numerical

1 INTRODUCTION

Chaos is regarded as a typical nonlinear phenomenon with exponential sensitivity on small variations of the initial conditions. Chaotic dynamics in classical physics has developed for about 40 years. However, its broad concern in relativistic astrophysics began only with the last decade or so.

Up to now, the study of chaos in general relativity has followed two main directions. One deals with the time evolution of a gravitational field itself, such as the dynamical evolution of mixmaster universe (Contopoulos et al. 1999; Hobill et al. 1994; Szydlowski 1997; Imponente & Montani 2001). The other concerns the geodesic or non-geodesic motion of particles in a given gravitational field. There are two types of typical physical models: spinning systems and static axisymmetric massive core-shell systems. Spinning systems, as the case of non-geodesic motion, mainly involve a spinning particle in Schwarzschild spacetime (Suzuki & Meada 1997), in Kerr spacetime (Hartl 2003) and spinning compact binaries (Hartl 2003; Levin 2000; Cornish 2001; Schnittman & Rasio 2001; Cornish & Levin 2002). It has been of particular interest to study the dynamics of spinning compact binaries because compact binary systems are an excellent natural source for investigating gravitational waves. Here it should be noted that gravitational wave detection can not succeed when chaos appears. On the other hand, many references focus on the geodesic motion of particles

* Supported by the National Natural Science Foundation of China.

in axisymmetric configurations called superposed Weyl spacetimes (Guéron & Letelier 2001, 2002; Vieira & Letelier 1999), which are viewed as idealized simplification models for many interesting astrophysical objects involving active galactic nuclei, black holes or neutron stars with axisymmetric surrounding sources such as accretion disks, massive halos, shells and rings. Certainly, the geodesic motion of other systems such as a celestial body with magnetic charge and moment is also considered (Wang & Huang 2001). One main interest lies in the survey of some physical properties and structures associated with fields, for example, conditions of the formation of static configuration, the motion of free test particles in the additional matter, etc (Semerák et al. 1999, 2001; Semerák & Žáček 2000; Karas 2004). Another motivation is to understand the dynamics of particles moving around superposed Weyl fields (Vieira & Letelier 1999). For the superposed Weyl field between a monopolar core and a pure halo dipole, there is a great contrast between Newtonian dynamics and its relativistic counterpart. Vieira & Letelier (1997) pointed out that the former is integrable, while the latter is chaotic in some cases. They explored further chaotic behaviors of orbits trapped in the intermediate vacuum between a core and shell of dipoles, quadrupoles, and octopoles (Vieira & Letelier 1999). In addition, the onset of chaos around the superposition of a black hole and a thin/thick disk can be seen in references (Saa & Venegeroles 1999; Saa 2000).

We emphasize that it would be questionable to apply Newtonian dynamical methods or indicators (such as Lyapunov exponents) for the identification of chaotic orbits from regular ones to a relativistic gravitational system. This is because time and space coordinates play only a bookkeeping role for events and have no physical meaning in general. Consequently, these indicators would not remain invariant under coordinate transformations in general relativity. There exists a widely known problem caused by non-covariant classical definition of Lyapunov exponents in mixmaster universe (Imponente & Montani 2001; Szydlowski et al. 1997). All these facts state that it is necessary to take a proper quantity rather than a coordinate one as an indicator for the detection of chaos in general relativity. To avoid the time coordinate redefinition ambiguity of Lyapunov exponents, Wu & Huang (2003) proposed a new definition (M1) of invariant Lyapunov exponents suitable for exploring the dynamics of orbits in relativistic gravitational systems with the help of a "1+3" splitting of spacetime and the projected norm. In fact, the definition is less rigorous in the framework of general relativity, and becomes only a revised version of the classical approximate two-particle method (Tancredi et al. 2001) for the computation of Lyapunov exponents. In view of this fact, Wu et al. (2005) presented a more rigorous method (M2) by means of geodesic deviation equations. In addition, another invariant two-particle method (M3) where the integration time variable in the geodesic equations is proper time rather than coordinate time, and the projected norm is not adopted. To check the validity of the two approximate methods M1 and M3, they compared M1 and M3 with M2 by choosing a static axisymmetric spacetime involving a Schwarzschild black hole plus a purely octopolar shell as a physical model. It is found that M2 might lead to overestimation of the Lyapunov exponents for either quasi-regular or chaotic orbits. The problem can be worked out through post-stabilization (Chin 1995) by variation of the 4-velocity constraint. Meanwhile, it is also pointed out that M1 fails to compute Lyapunov exponents when the time component of the 4-velocity of an observer (i.e. a reference trajectory) is always larger than 1 at any proper time of the observer, and the difference in coordinate time and his proper time becomes dramatic viewed on a long time. As a result, M3 was recommended for most cases.

In the present paper, the geodesic equations and their geodesic deviation equations for a Weyl spacetime are derived in detail, and some details as to how to solve the geodesic deviation vector numerically by post-stabilization are given. Another important motivation is to find a simple and fast method to estimate the effects of different parameters on the dynamical features of the black-hole + octopolar-shell system. In this sense, fast Lyapunov indicators (Froeschlé et al. 1997), as a very sensitive tool to separate chaotic from regular orbits, are adopted. The paper is organized as follows. Some details of the previous paper are given in Section 2. By virtue of the Poincaré surface of section and the Lyapunov exponents, we explore the dynamics of this system numerically in Section 3. In Section 4 we use fast Lyapunov indicators to gain further insight into the dynamics of the particles in the spacetime for various dynamical parameters. Finally, a summary follows in Section 5. Some complicated expressions are listed in an Appendix.

2 SOME DETAILS OF THE PREVIOUS WORK

Suppose that a particle moves freely in a four-dimensional time-like spacetime with the metric $ds^2 = g_{\mu\nu}dx^\mu dx^\nu$, where Greek subscripts run from 0 to 3 and Latin indexes from 1 to 3, and $c = G = 1$ units are used. Its equations of motion are the following geodesic equations:

$$\ddot{x}^\mu = -\Gamma^\mu_{\alpha\beta}\dot{x}^\alpha\dot{x}^\beta\,, \tag{1}$$

and the corresponding geodesic deviation equations are

$$\frac{D^2\xi^\mu}{D\tau^2} = -R^\mu_{\alpha\lambda\beta}\xi^\lambda U^\alpha U^\beta\,. \tag{2}$$

Equation (2) can be rewritten in the form

$$\ddot{\xi}^\mu = -2\Gamma^\mu_{\alpha\beta}\dot{\xi}^\beta U^\alpha - \Gamma^\mu_{\alpha\beta,\lambda}\xi^\lambda U^\alpha U^\beta\,. \tag{3}$$

In the above expressions, $\Gamma^\mu_{\alpha\beta}$ is a Christoffel symbol, and $R^\mu_{\alpha\lambda\beta}$ denotes a Riemannian curvature tensor, U^α, ξ^μ and $\dot{\xi}^\mu$ stand for the 4-velocity, the geodesic deviation vector and its derivative, respectively.

Next, we will write down the concrete expressions of geodesic equations and their geodesic deviation equations for a static axisymmetric spacetime, namely, a Weyl spacetime.

2.1 Geodesic Equations and Geodesic Deviation Equations for a Weyl Metric

Let us consider a black-hole-shell configuration, which comprises a central black hole surrounded by an axisymmetric shell. The vacuum between the core and the shell can be described by the Weyl spacetime (Vieira & Letelier 1999)

$$ds^2 = -\Big(1-\frac{2}{r}\Big)e^P dt^2 + e^{Q-P}\Big[\Big(1-\frac{2}{r}\Big)^{-1}dr^2 + r^2 d\theta^2\Big] + e^{-P}r^2\sin^2\theta d\phi^2\,, \tag{4}$$

where (t, r, θ, ϕ) is a set of Schwarzchild coordinates, while P and Q are two functions depending on r and θ only. P relates to the gravitational potential of the shell, and Q deals with the nonlinear coupling interaction between the core and the shell besides a potential from the shell. P and Q are expressed as sums of multipoles. Obviously Eq. (4) represents the Schwarzchild spacetime if there exists no shell-type matter.

It is easy to find two integrals, namely, the specific energy constant E and specific angular momentum constant L in the ϕ direction:

$$\dot{t} = Er(r-2)^{-1}e^{-P}, \tag{5}$$

$$\dot{\phi} = Le^P r^{-2}\sin^{-2}\theta\,. \tag{6}$$

For the 4-velocity U^α, there is always the identity,

$$U_\alpha U^\alpha = -\Big(1-\frac{2}{r}\Big)e^P\dot{t}^2 + e^{Q-P}\Big[\Big(1-\frac{2}{r}\Big)^{-1}\dot{r}^2 + r^2\dot{\theta}^2\Big] + e^{-P}r^2\sin^2\theta\dot{\phi}^2 = -1\,. \tag{7}$$

Thus we have the three obvious integrals above.

If a fourth integral exists, then the integrability of the spacetime is ensured. Otherwise, chaos becomes possible. In general, it is difficult to judge whether or not there is a fourth integral. For more information with regard to the dynamical behavior of the spacetime, it is necessary to use the geodesic equations, even the geodesic deviation equations. Because the evolution equations about t and ϕ have been given by the first-order ordinary differential Eqs. (5) and (6) respectively, in the light of Eq. (1) we consider only the evolution equations of r and θ in the forms

$$\ddot{r} = -(\Gamma^1_{00}\dot{t}^2 + \Gamma^1_{11}\dot{r}^2 + 2\Gamma^1_{12}\dot{r}\dot{\theta} + \Gamma^1_{22}\dot{\theta}^2 + \Gamma^1_{33}\dot{\phi}^2)\,, \tag{8}$$

$$\ddot{\theta} = -(\Gamma^2_{00}\dot{t}^2 + \Gamma^2_{11}\dot{r}^2 + 2\Gamma^2_{12}\dot{r}\dot{\theta} + \Gamma^2_{22}\dot{\theta}^2 + \Gamma^2_{33}\dot{\phi}^2)\,. \tag{9}$$

Noting Eq. (3), we can write the geodesic deviation equations

$$\delta\dot{t} = -2(\Gamma^0_{01}\dot{t}\delta r + \Gamma^0_{02}\dot{t}\delta\theta)\,, \tag{10}$$

$$\delta\dot{\phi} = -2(\Gamma^3_{13}\dot{\phi}\delta r + \Gamma^3_{23}\dot{\phi}\delta\theta)\,, \tag{11}$$

$$\begin{aligned}\delta\ddot{r} = {} & -2(\Gamma^1_{00}\dot{t}\delta\dot{t} + \Gamma^1_{11}\dot{r}\delta\dot{r} + \Gamma^1_{12}\dot{r}\delta\dot{\theta} + \Gamma^1_{21}\dot{\theta}\delta\dot{r} + \Gamma^1_{22}\dot{\theta}\delta\dot{\theta} + \Gamma^1_{33}\dot{\phi}\delta\dot{\phi}) \\ & -(\Gamma^1_{00,1}\dot{t}^2\delta r + \Gamma^1_{00,2}\dot{t}^2\delta\theta + \Gamma^1_{11,1}\dot{r}^2\delta r + \Gamma^1_{11,2}\dot{r}^2\delta\theta + 2\Gamma^1_{12,1}\dot{r}\dot{\theta}\delta r \\ & +2\Gamma^1_{12,2}\dot{r}\dot{\theta}\delta\theta + \Gamma^1_{22,1}\dot{\theta}^2\delta r + \Gamma^1_{22,2}\dot{\theta}^2\delta\theta + \Gamma^1_{33,1}\dot{\phi}^2\delta r + \Gamma^1_{33,2}\dot{\phi}^2\delta\theta),\end{aligned} \tag{12}$$

$$\begin{aligned}\delta\ddot{\theta} = {} & -2(\Gamma^2_{00}\dot{t}\delta\dot{t} + \Gamma^2_{11}\dot{r}\delta\dot{r} + \Gamma^2_{12}\dot{r}\delta\dot{\theta} + \Gamma^2_{21}\dot{\theta}\delta\dot{r} + \Gamma^2_{22}\dot{\theta}\delta\dot{\theta} + \Gamma^2_{33}\dot{\phi}\delta\dot{\phi}) \\ & -(\Gamma^2_{00,1}\dot{t}^2\delta r + \Gamma^2_{00,2}\dot{t}^2\delta\theta + \Gamma^2_{11,1}\dot{r}^2\delta r + \Gamma^2_{11,2}\dot{r}^2\delta\theta + 2\Gamma^2_{12,1}\dot{r}\dot{\theta}\delta r \\ & +2\Gamma^2_{12,2}\dot{r}\dot{\theta}\delta\theta + \Gamma^2_{22,1}\dot{\theta}^2\delta r + \Gamma^2_{22,2}\dot{\theta}^2\delta\theta + \Gamma^2_{33,1}\dot{\phi}^2\delta r + \Gamma^2_{33,2}\dot{\phi}^2\delta\theta).\end{aligned} \tag{13}$$

As an illustration, Eqs. (10) and (11) are derived from the variations of Eqs. (5) and (6) rather than Eq. (3). The relevant non-vanishing Christoffel symbols associated with their partial derivatives are displayed in Appendix A.

It is obvious that the geodesic Eqs. (5), (6), (8) and (9) as well as the geodesic deviation equations (10)–(13) are not easy to solve exactly and that one has no choice but numerical integrations. However, the usual integrators bring on some artificial dissipation in long-term integrations. This may lead to a destruction of some constraints so great that the numerical solutions become meaningless. As was stated in the previous work (Wu et al. 2005), the Runge-Kutta-Fehlberg (9) 8 (hereafter RKF(9)8) scheme displays such a bad numerical accuracy of the geodesic deviation vector that spurious Lyapunov exponents occur, and it was recommended post-stabilization be used with the integrator to preserve the constraints. The following subsection gives some details of the implementation of post-stabilization.

2.2 To Solve the Geodesic Deviation Equations Numerically by Use of the Post-stabilization

2.2.1 Some Constraints

In fact, the variables t, ϕ, $\dot{t}$, $\dot{\phi}$, δt, $\delta\phi$, $\delta\dot{t}$ and $\delta\dot{\phi}$ do not explicitly appear in the four second-order differential Equations (8), (9), (12) and (13) through rearrangement. Thus these four equations should have been separated into eight first-order differential equations in the variables, r, θ, $\dot{r}$, $\dot{\theta}$, δr, $\delta\theta$, $\delta\dot{r}$ and $\delta\dot{\theta}$. However, only six of these variables are independent owing to the existence of the 4-velocity constraint (7) and its variational constraint $\delta(U_\alpha U^\alpha) = 0$. It is a practical problem as to how to compute constrained systems numerically. In principle, the number of numerically integrated first-order differential equations should be the same as the dimension of the phase space. It means that two variables, e.g., $\dot{\theta}$ and $\delta\dot{\theta}$, should be removed. This idea is called reduction of the order of differential equations of motion by use of constraints (Wu & Huang 2005).

As far as the constraint (7) is concerned, we have

$$\dot{\theta} = \pm\sqrt{r^{-2}e^{P-Q}\Big[-1 + \Big(1-\frac{2}{r}\Big)e^P\dot{t}^2 - e^{Q-P}\Big(1-\frac{2}{r}\Big)^{-1}\dot{r}^2 - e^{-P}r^2\sin^2\theta\dot{\phi}^2\Big]}. \tag{14}$$

It is difficult to choose the signs in the course of numerical integration, therefore, we do not succeed in removing the $\dot{\theta}$ variable. In other words, the reduction of the order of equations becomes invalid in this case. In spite of this, $\dot{\theta}$ should be given by Eq. (14) at the initial time, and it is admissible to select arbitrarily one of the two signs.

On the other hand, the variational constraint of 4-velocity is

$$\begin{aligned}\delta U \;=\; & -e^{P}\dot{t}^{2}\Big[\frac{2}{r^{2}}\delta r+\Big(1-\frac{2}{r}\Big)\Big(\frac{\partial P}{\partial r}\delta r+\frac{\partial P}{\partial\theta}\delta\theta\Big)+\Big(1-\frac{2}{r}\Big)\frac{2}{\dot{t}}\Big(\frac{\partial\dot{t}}{\partial r}\delta r+\frac{\partial\dot{t}}{\partial\theta}\delta\theta\Big)\Big]+e^{Q-P}\\ & \cdot\Big\{\Big[\Big(\frac{\partial Q}{\partial r}-\frac{\partial P}{\partial r}\Big)\delta r+\Big(\frac{\partial Q}{\partial\theta}-\frac{\partial P}{\partial\theta}\Big)\delta\theta\Big]\cdot\Big[\Big(1-\frac{2}{r}\Big)^{-1}\dot{r}^{2}+r^{2}\dot{\theta}^{2}\Big]-\frac{2}{r^{2}}\Big(1-\frac{2}{r}\Big)^{-2}\dot{r}^{2}\delta r\\ & +2\Big(1-\frac{2}{r}\Big)^{-1}\dot{r}\delta\dot{r}+2r\dot{\theta}^{2}\delta r+2r^{2}\dot{\theta}\delta\dot{\theta}\Big]\Big\}+e^{-P}r^{2}\sin^{2}\theta\dot{\phi}^{2}\Big[-\frac{\partial P}{\partial r}\delta r-\frac{\partial P}{\partial\theta}\delta\theta+\frac{2}{r}\delta r\\ & +2\frac{\cos\theta}{\sin\theta}\delta\theta+\frac{2}{\dot{\phi}}\Big(\frac{\partial\dot{\phi}}{\partial r}\delta r+\frac{\partial\dot{\phi}}{\partial\theta}\delta\theta\Big)\Big]=0,\end{aligned}\tag{15}$$

where δU is a linear function of δr, $\delta\theta$, $\delta\dot{r}$ and $\delta\dot{\theta}$. We easily solve for $\delta\dot{\theta}$ and obtain

$$\begin{aligned}\delta\dot{\theta} \;=\; & e^{2P-Q}\dot{t}^{2}(2r^{2}\dot{\theta})^{-1}\Big[\frac{2}{r^{2}}\delta r+\Big(1-\frac{2}{r}\Big)\Big(\frac{\partial P}{\partial r}\delta r+\frac{\partial P}{\partial\theta}\delta\theta\Big)+\Big(1-\frac{2}{r}\Big)\frac{2}{\dot{t}}\Big(\frac{\partial\dot{t}}{\partial r}\delta r+\frac{\partial\dot{t}}{\partial\theta}\delta\theta\Big)\Big]\\ & -(2r^{2}\dot{\theta})^{-1}\cdot\Big\{\Big[\Big(\frac{\partial Q}{\partial r}-\frac{\partial P}{\partial r}\Big)\delta r+\Big(\frac{\partial Q}{\partial\theta}-\frac{\partial P}{\partial\theta}\Big)\delta\theta\Big]\cdot\Big[\Big(1-\frac{2}{r}\Big)^{-1}\dot{r}^{2}+r^{2}\dot{\theta}^{2}\Big]\\ & -\frac{2}{r^{2}}\Big(1-\frac{2}{r}\Big)^{-2}\dot{r}^{2}\delta r+2\Big(1-\frac{2}{r}\Big)^{-1}\dot{r}\delta\dot{r}+2r\dot{\theta}^{2}\delta r\Big]\Big\}-e^{-Q}\sin^{2}\theta\dot{\phi}^{2}(2\dot{\theta})^{-1}\\ & \cdot\Big[-\frac{\partial P}{\partial r}\delta r-\frac{\partial P}{\partial\theta}\delta\theta+\frac{2}{r}\delta r+2\frac{\cos\theta}{\sin\theta}\delta\theta+\frac{2}{\dot{\phi}}\Big(\frac{\partial\dot{\phi}}{\partial r}\delta r+\frac{\partial\dot{\phi}}{\partial\theta}\delta\theta\Big)\Big].\end{aligned}\tag{16}$$

It seems advantageous to implement the reduction of the order of equations if we adopt Eq. (12) with Eq. (16) instead of Eq. (13) to work out the variational solution ($\delta r, \delta\theta, \delta\dot{r}$, and $\delta\dot{\theta}$). However, $\dot{\theta}$ may be equal to zero at some time when the integration scheme would fail.

As was mentioned in the previous work, Baumgarte's stabilization method (1973) or Chin's post-stabilization method (1995) is a simpler way for the conservation of one or more constraints during the whole numerical integration.

2.2.2 Post-stabilization

A constraint is also called a control term or a stabilizing term. Baumgarte's method (1973) is called stabilization of differential equations where the differential equations to be integrated numerically are modified by adding the control term. Avdyushev (2003) discussed it further. To avoid encountering difficulty in choosing the best stabilizing parameters, we are particularly interested in Chin's post-stabilization method (1995) among the different stabilization methods. The kernel of post-stabilization is to add a control term to the numerical solution at the end of each time step; the control term is obtained from a generic numerical method applied to the original equations of motion. In detail, the process is as follows: (i) suppose that a first-order system $\dot{\boldsymbol{x}}=\boldsymbol{f}(\boldsymbol{x})$ has the approach solution $\boldsymbol{x}_n$ at time t_n, and then its numerical solution $\boldsymbol{x}_{n+1}$ at time t_{n+1} is worked out by using a certain given integration scheme; (ii) the numerical solution $\boldsymbol{x}_{n+1}$ should be demanded to be corrected to the constraint supersurface by

$$\hat{\boldsymbol{x}}_{n+1}\leftarrow\boldsymbol{x}_{n+1}-\Phi\frac{\partial\Phi}{\partial\boldsymbol{x}}\Big/\Big(\frac{\partial\Phi}{\partial\boldsymbol{x}}\circ\frac{\partial\Phi}{\partial\boldsymbol{x}}\Big)\Big|_{\boldsymbol{x}=\boldsymbol{x}_{n+1}},\tag{17}$$

where '$\circ$' is the Euclidian inner product. By repeating the above operation, an approximate numerical solution sequence $\{\hat{\boldsymbol{x}}_n\}$ is obtained. For more details, see the references (Chin 1995; Zhang 1996; Ascher 1997; Wu et al. 2006).

In Eq. (17) Φ stands for the control term. It is better to choose the energy integral as the stabilizing term for an autonomous Hamiltonian system $H(\boldsymbol{q},\boldsymbol{p})$, namely $\Phi=\Delta H=H-H_0$, where H_0 stands for the initial energy. Then Eq. (17) appears in the following concrete forms

$$\hat{\boldsymbol{q}}_{n+1} \;=\; \boldsymbol{q}_{n+1}-\frac{\Delta H\cdot H_{\boldsymbol{q}}}{H_{\boldsymbol{q}}\circ H_{\boldsymbol{q}}+H_{\boldsymbol{p}}\circ H_{\boldsymbol{p}}}(\boldsymbol{q}_{n+1},\boldsymbol{p}_{n+1}),$$

$$\hat{\boldsymbol{p}}_{n+1} = \boldsymbol{p}_{n+1} - \frac{\Delta H \cdot H_{\boldsymbol{p}}}{H_{\boldsymbol{q}} \circ H_{\boldsymbol{q}} + H_{\boldsymbol{p}} \circ H_{\boldsymbol{p}}}(\boldsymbol{q}_{n+1}, \boldsymbol{p}_{n+1}),$$

where $H_{\boldsymbol{q}} = \frac{\partial H}{\partial \boldsymbol{q}}$ and $H_{\boldsymbol{p}} = \frac{\partial H}{\partial \boldsymbol{p}}$.

2.2.3 Post-stabilization by Constraints for a Geodesic Flow

For the geodesic motion (4), we should choose the 4-velocity constraint (7) as the control term without any hesitation. First, we adopt a traditional integrator to integrate Eqs. (8) and (9) so that we can obtain the numerical solution $(r, \theta, \dot{r}, \dot{\theta})$. Then, by use of the constraint $\Delta U = U_\alpha U^\alpha + 1$, the numerical solution is corrected with the forms

$$\begin{aligned} \hat{r} &= r - \frac{\Delta U}{UU}\frac{\partial \Delta U}{\partial r}, \qquad \hat{\theta} = \theta - \frac{\Delta U}{UU}\frac{\partial \Delta U}{\partial \theta}, \\ \hat{\dot{r}} &= \dot{r} - \frac{\Delta U}{UU}\frac{\partial \Delta U}{\partial \dot{r}}, \qquad \hat{\dot{\theta}} = \dot{\theta} - \frac{\Delta U}{UU}\frac{\partial \Delta U}{\partial \dot{\theta}}, \\ UU &= \Big(\frac{\partial \Delta U}{\partial r}\Big)^2 + \Big(\frac{\partial \Delta U}{\partial \theta}\Big)^2 + \Big(\frac{\partial \Delta U}{\partial \dot{r}}\Big)^2 + \Big(\frac{\partial \Delta U}{\partial \dot{\theta}}\Big)^2. \end{aligned} \tag{18}$$

Here the partial derivatives are

$$\begin{aligned} \frac{\partial \Delta U}{\partial r} &= -e^P \dot{t}^2 \Big[\frac{2}{r^2} + \Big(1 - \frac{2}{r}\Big)\Big(\frac{\partial P}{\partial r} + \frac{2}{\dot{t}}\frac{\partial \dot{t}}{\partial r}\Big)\Big] + e^{Q-P}\Big\{\Big(\frac{\partial Q}{\partial r} - \frac{\partial P}{\partial r}\Big)\Big[\Big(1 - \frac{2}{r}\Big)^{-1}\dot{r}^2 + r^2\dot{\theta}^2\Big] \\ &\quad -\frac{2}{r^2}\Big(1 - \frac{2}{r}\Big)^{-2}\dot{r}^2 + 2r\dot{\theta}^2\Big\} + e^{-P} r^2 \sin^2\theta \dot{\phi}^2 \cdot \Big(-\frac{\partial P}{\partial r} + \frac{2}{r} + \frac{2}{\dot{\phi}}\frac{\partial \dot{\phi}}{\partial r}\Big), \\ \frac{\partial \Delta U}{\partial \theta} &= -e^P \dot{t}^2 \Big(1 - \frac{2}{r}\Big)\Big(\frac{\partial P}{\partial \theta} + \frac{2}{\dot{t}}\frac{\partial \dot{t}}{\partial \theta}\Big) + e^{Q-P}\Big(\frac{\partial Q}{\partial \theta} - \frac{\partial P}{\partial \theta}\Big)\Big[\Big(1 - \frac{2}{r}\Big)^{-1}\dot{r}^2 + r^2\dot{\theta}^2\Big] \\ &\quad + e^{-P} r^2 \sin^2\theta \dot{\phi}^2\Big(-\frac{\partial P}{\partial \theta} + 2\frac{\cos\theta}{\sin\theta} + \frac{2}{\dot{\phi}}\frac{\partial \dot{\phi}}{\partial \theta}\Big), \\ \frac{\partial \Delta U}{\partial \dot{r}} &= 2\dot{r} e^{Q-P}\Big(1 - \frac{2}{r}\Big)^{-1}, \qquad \frac{\partial \Delta U}{\partial \dot{\theta}} = 2r^2\dot{\theta} e^{Q-P}. \end{aligned}$$

As an illustration, $\partial \dot{t}/\partial r = -2\Gamma^0_{01}\dot{t}$, $\partial \dot{t}/\partial \theta = -2\Gamma^0_{02}\dot{t}$, $\partial \dot{\phi}/\partial r = -2\Gamma^3_{13}\dot{\phi}$ and $\partial \dot{\phi}/\partial \theta = -2\Gamma^3_{23}\dot{\phi}$. The corrected solution is taken as new initial conditions and the above procedure is repeated.

In the same way, we treat the variational solution by

$$\begin{aligned} \delta\hat{r} &= \delta r - \frac{\delta U}{UU}\frac{\partial \Delta U}{\partial r}, \qquad \delta\hat{\theta} = \delta\theta - \frac{\delta U}{UU}\frac{\partial \Delta U}{\partial \theta}, \\ \delta\hat{\dot{r}} &= \delta\dot{r} - \frac{\delta U}{UU}\frac{\partial \Delta U}{\partial \dot{r}}, \qquad \delta\hat{\dot{\theta}} = \delta\dot{\theta} - \frac{\delta U}{UU}\frac{\partial \Delta U}{\partial \dot{\theta}}. \end{aligned} \tag{19}$$

Then we take the corrected variational solution as the initial conditions for the next integration, and so on.

As an important application, the corrected variational solution is used to compute the Lyapunov exponents.

2.3 Lyapunov Exponents

In classical physics, Lyapunov exponents are a key indicator of the mean exponential rate of divergence of two nearby trajectories. One rigorous method for computing the Lyapunov exponents is to use the tangent vector from the solution of the variational equations of the system. Another less rigorous method is the so-called two-particle method (Tancredi et al. 2001), where we use the deviation vector between two nearby trajectories (one the reference, one, the shadow) in place of the tangent vector. For a compact system, the system is said to be regular if the maximum

Lyapunov exponent equals zero, and chaotic if a Lyapunov exponent is positive. Although Lyapunov exponents are defined in the phase space, it is preferable to compute the Lyapunov exponents in the configuration space; the Lyapunov exponents in the two spaces are equivalent in detecting the long-term dynamical behavior of orbits (Wu & Huang 2003). We shall be computing the Lyapunov exponents in the configuration space for preference.

As is well-known, the definition of Lyapunov exponents in Newtonian mechanics is not invariant under coordinate transformations in general relativity. In this sense, it is vital to refine the classical definition according to the requirement of coordinate gauge invariance. Three invariant methods of computing the Lyapunov exponents were stated in the previous work. Here we give one of three methods, i.e. the rigorous method (called "M2" in the Introduction) by the geodesic deviation vector. In fact, it is easy to obtain the relativistic method from the classical variational method when the geodesic deviation vector $\boldsymbol{\xi}$, the Riemannian norm and the proper time τ are used in place of the tangent vector, the Euclidian norm and the coordinate time t, respectively, for the maximum invariant Lyapunov exponent can then be written as

$$\Lambda = \lim_{\tau\to\infty} \frac{1}{\tau} \log \frac{\|\boldsymbol{\xi}(\tau)\|}{\|\boldsymbol{\xi}(0)\|}, \tag{20}$$

where the Riemannian norm $\|\boldsymbol{\xi}(\tau)\| = \sqrt{|\boldsymbol{\xi}\cdot\boldsymbol{\xi}|} = \sqrt{|g_{\mu\nu}\xi^\mu\xi^\nu|}$. For a given geodesic flow, the Riemannian inner product $\boldsymbol{\xi}\cdot\boldsymbol{\xi}$ is positive definite due to the $\boldsymbol{\xi}$ being space-like. Of course, the method is too cumbersome to be given in many cases because of the complicated derivation of the geodesic deviation equations. However, it is meaningful to use the method as a reference standard to check the validity of other approximate methods.

To study the dynamics of orbits in a black-hole + octopolar-shell field further, we apply the Lyapunov exponent given by Eq. (20) with Poincaré surface of section to the system. We are concerned above all with the difference in the computation of Lyapunov exponents with and without post-stabilization.

3 NUMERICAL EXPLORATIONS OF A SUPERPOSED FIELD BETWEEN A BLACK HOLE AND AN OCTOPOLAR SHELL

Let us re-examine the full relativistic core-shell configuration involving a Schwarzschild black hole plus a pure octopole with two metric functions (Vieira & Letelier 1999)

$$\begin{aligned} P(u,v) &= \frac{1}{5}\mathcal{O}uv(5u^2-3)(5v^2-3), \\ Q(u,v) &= -\frac{2}{5}\mathcal{O}v[5(3u^2-1)(1-v^2)-4] + \frac{3}{100}\mathcal{O}^2[-25u^6(1-v^2) \\ &\quad \cdot(5v^2+2v-1)(5v^2-2v-1) + 15u^4(1-v^2)(65v^4-40v^2+3) \\ &\quad -3u^2(1-v^2)(25v^2-3)(5v^2-3) - v^2(25v^4-45v^2+27)], \end{aligned}$$

where $u = r-1$, $v = \cos\theta$, and $\mathcal{O}$ is an octopolar parameter.

Unlike the previous work, here we adopt distinct dynamical parameters and starting conditions. Let the angular momentum L be equal to 3.8, and the other dynamical parameters be $E = 0.9675$ and $\mathcal{O} = 7.25\times10^{-7}$ instead of $E = 0.9679$ and $\mathcal{O} = 7.012\times10^{-7}$. The initial values of three variables, r, θ and $\dot{r}$, can be given arbitrarily in their respective admissive intervals, but $\dot{\theta}$ must obey Eq. (14) at the initial time. As a check, some of orbits satisfying the geodesic Eqs. (8) and (9) were computed independently by each of us, using different integration schemes (RKF(9)8 and the 12th order Adams-Cowell integrator). The Poincaré surface of section at the plane $\theta = \pi/2$, $\dot{\theta} < 0$ shown in the left of Figure 1 was obtained using RKF(9)8. The global dynamical structure of the system (4) can be clearly seen from the surface of section. Orbits in the $(r,\dot{r})$ plane are classified as either regular orbits or chaotic orbits. There is a larger region consisting of many tori and islands, which correspond to regular orbits. Each torus can be obtained from a point in the Poincaré map. For example, mapping the starting point $F(10,-0.05)$ in the $(r,\dot{r})$ plane, we acquire a set of points F_i that lie precisely on a single torus. Here no points F_i will come back exactly to the starting point F,

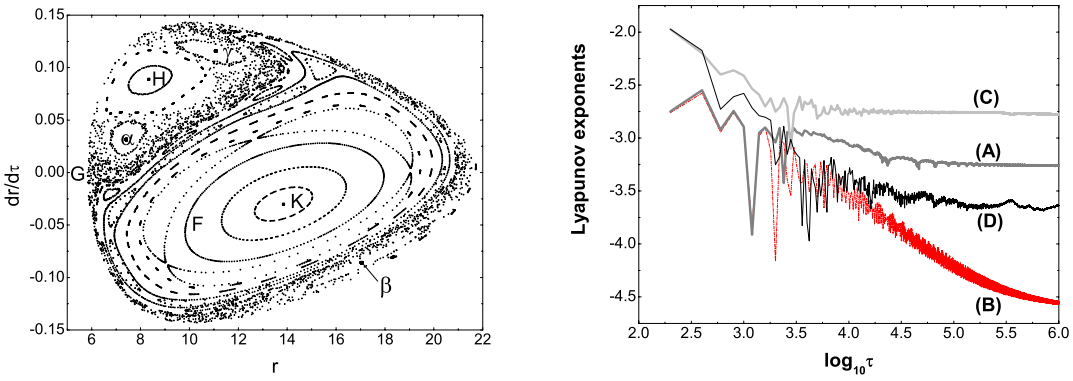

Fig. 1 Left: Poincaré surface of section at the plane $\theta = \pi/2$, $\dot{\theta} < 0$ for the full relativistic core-shell configuration with parameters $E = 0.9675$, $L = 3.8$ and $\mathcal{O} = 7.25 \times 10^{-7}$. Right: Maximum Lyapunov exponent as a function of integration time for the regular orbit with the starting point $F(10, -0.05)$ in the $(r, \dot{r})$ plane (Curves A and B) and for the chaotic orbit with the initial point $G(6.5, 0)$ (Curves C and D). Curves (A) and (C) are integrated simply with RKF(9)8; Curves (B) and (D) resulted from integration with post stabilization by the variational constraint of the 4-velocity. Common logarithmic scale is used for both axes.

and the infinite set of the points F_i is dense everywhere on the torus. It means that the trajectory in the phase space is not closed. In the case, the trajectory is typically quasi-periodic. For the trajectory made up of the three little loops or islands surrounding three points $\alpha(7.415, 0.0315)$, $\beta(17.042, -0.0857)$ and $\gamma(11.071, 0.1159)$, respectively, an important point to emphasize is the manner in which the three little loops appear on the plot as the same trajectory. Rather than tracing out one loop at a time, successive points occur at each of the three loops locations in turn. Hénon & Heiles (1964) called this feature a *chain of islands*. There are other such chains in the diagram, but some of them can be invisible if the islands are too small. The existence of tori or chains means the presence of other isolating integrals for the system. In the middle of the tori there are two invariant points $H(8.341, 0.0889)$ and $K(13.846, -0.0301)$ of the Poincaré map. They correspond to independent stable and closed periodic orbits. These periodic orbits may be elliptical orbits in the three-dimensional configuration space, but they can not be circular orbits because the stability criterion of a circular orbit is the *effective potential* is an extremum at the point H or K. Similarly, three fixed points, α, β and γ, at the centers of the chain of three islands, are said to be periodic points of the Poincaré map in that the system returns to the same point every third time the orbit crosses the section. On the other hand, mapping the starting point $G(6.5, 0)$, we have a number of isolated points, which are randomly distributed in a smaller region called a chaotic region.

Also we use the Lyapunov exponent by Eq. (20) to investigate the orbital dynamics of particles in the spacetime quantitatively. To obtain the geodesic deviation vector $\boldsymbol{\xi}$, we have to integrate Eqs. (5), (6), and (8)–(13) together numerically. Furthermore, it is necessary to apply a periodic renormalization to avoid overflow due to fast growth of $\boldsymbol{\xi}$. Although the Lyapunov exponents are defined in the configuration space, the renormalization should be limited to the phase space, that is, the velocity deviation vector $\dot{\boldsymbol{\xi}}(t)$ should be multiplied by the same factor $1/\|\boldsymbol{\xi}(t)\|$ as when the deviation vector $\boldsymbol{\xi}(t)$ is pulled back from its unit vector. In addition, we take the proper time τ as the integration variable, and assume at $t = 0$, the initial values $\theta = \pi/2$, $\phi = 0$, $\delta t = 0$, $\delta r = 1/\sqrt{g_{11}}$, $\delta\theta = 0$, $\delta\phi = 0$ and $\delta\dot{r} = 0$. The initial values of $\dot{\theta}$ and $\delta\dot{\theta}$ are given by Eqs. (14) and (16), and the initial values of r and $\dot{r}$ are provided in the different cases.

Curve (A) in the right of Figure 1 displays the maximum Lyapunov exponent for a regular orbit with the initial point F. As the previous work mentioned, we can see again that there is a fully false estimation of a positive value. A tentative interpretation of this overestimation stems from a breakdown of the variational constraint (15) due to insufficient accuracy in the course of the numerical integration. It was reported that this problem could be successfully treated with post-stabilization. Accordingly, we took Eq. (19) and recalculated the Lyapunov exponent for the same orbit. As is shown by Curve (B) in the right of Figure 1, the Lyapunov exponent now tends to zero. Here the superiority of the post-stabilization is dramatically visible. In contrast, the problem of spurious Lyapunov exponent remains if we use Eq. (18) in place of Eq. (19). The reason is that RKF(9)8 has maintained the 4-velocity constraint (7) with a rather higher accuracy so that the numerical solution of the geodesic equations is not necessarily corrected by the post-stabilization. Otherwise, Eqs. (18) and (19) should be used together if Eq. (20) is used to calculate the Lyapunov exponents.

Repeating the above procedure, we followed a chaotic orbit with the starting point G. The case is similar to the above. Specifically, without post-stabilization, a spurious large value of the Lyapunov exponent appears (see curves (C) and (D) in the right of Fig. 1). This shows once again the superiority of post-stabilization.

The above facts have amply demonstrated that post-stabilization brings about a better numerical accuracy. The treatment is not more expensive and is simple to use: it is an interesting technique to compute the Lyapunov exponents that tell us information on the dynamical behavior of the orbits. Now we wonder what the dynamical properties at the fixed points α (or β and γ), H and K of the Poincaré map are when we vary the dynamical parameters. However, it is very expensive to obtain a stable limit value of the Lyapunov exponent. So, it is an advantage to use the fast Lyapunov indicators (Froeschlé et al. 1997).

4 ASSESSMENT OF EFFECTS OF DISTINCT PARAMETERS ON DYNAMICAL FEATURES USING FAST LYAPUNOV INDICATORS

4.1 Fast Lyapunov Indicators

It is well known that the time necessary to reach a given value, either of the length of any tangential vector or of the angle between tangential vectors is taken as an indicator of stochasticity for a Newtonian dynamical system. Following this general idea Froeschlé et al. (1997) defined three different fast Lyapunov indicators as follows:

$$\psi_1(t) \;=\; 1/|\boldsymbol{v}_1(t)|^n\,, \tag{21}$$

$$\psi_2(t) \;=\; 1/(\prod_{j=1}^{n} |\boldsymbol{v}_j(t)|)\,, \tag{22}$$

$$\psi_3(t) \;=\; 1/(sup_j|\boldsymbol{v}_j(t)|^n)\,. \tag{23}$$

Here $\boldsymbol{V}_n(0) = (\boldsymbol{v}_1(0), \boldsymbol{v}_2(0), \cdots, \boldsymbol{v}_n(0))$ is a set of n independent vectors in an n-dimensional phase space with the same initial condition $\boldsymbol{X}_n(0) = (x_1(0), x_2(0), \cdots, x_n(0))$, the symbol "| |" denotes the Euclidian norm, and $\boldsymbol{v}_j(t)$ represents the *j-th* tangential vector at time t. It is particularly emphasised that no renormalization is made at all in the whole course of integration of the variational equations. Given any threshold, any one of the three indicators will reach the value fast for a chaotic orbit, and slowly for a regular orbit. Conversely, in the same time span, any one of these indicators will tend to show different values for an ordered and a chaotic orbit with completely different time rates. More specifically, each of the three indicators will decrease exponentially with time for a chaotic orbit, while only polynomially for an ordered orbit. This allows one to distinguish between the two cases. Because the computation of two indicators $\psi_2(t)$ and $\psi_3(t)$ requires solving of the variational equations for n times for a set of n initial tangential vectors, it would no longer be cheap. Froeschlé & Lega (2000) therefore gave a fourth indicator of the form

$$\psi_4(t) = \log|\boldsymbol{v}_1(t)|\,. \tag{24}$$

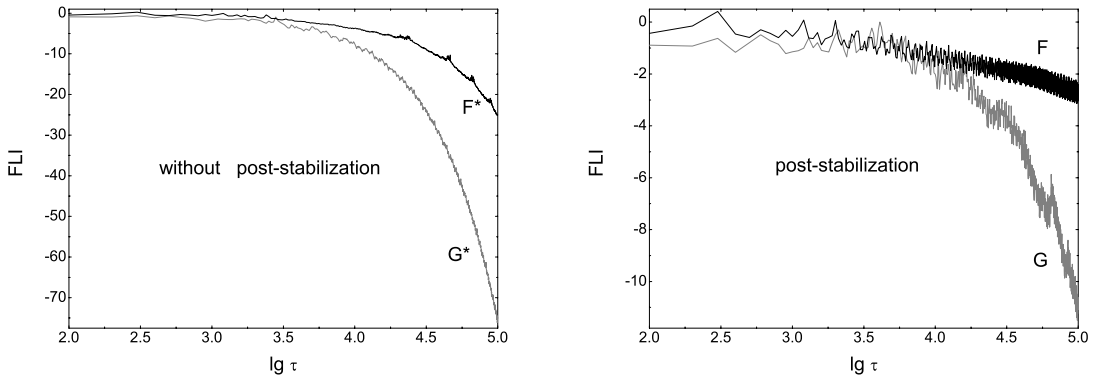

Fig. 2 Decay of the FLI with proper time τ. Curve F is for the regular orbit with the starting point F; Curve G, the chaotic orbit with the initial point G. Curves marked with the asterisk are cases where post-stabilization by the constraint (15) was not applied.

This expression describes the evolution of the separation between two nearby trajectories with time. It is clear that the indicator $\psi_4(t)$ divided by a sufficiently long time t is the maximum Lyapunov exponent for the case of an initial unit vector. On the other hand, $\psi_4(t)$ is regarded as the largest Lyapunov exponent in a relatively short time. This shows their correlation. Compared with the Lyapunov exponent, $\psi_4(t)$ is a faster and more sensitive tool for discriminating between ordered and weakly chaotic motion.

Now let us apply a fast Lyapunov indicator to the relativistic gravitational system (4). As in the case of Lyapunov exponent, it is necessary to avoid the lack of covariance. Accordingly, we have to modify the fast Lyapunov indicator (FLI) with the following expression,

$$\mathrm{FLI}(\tau) = -\lg \|\boldsymbol{\xi}(\tau)\|\,, \tag{25}$$

in the light of Eqs. (21) and (24). Here $\boldsymbol{\xi}$ satisfies the geodesic deviation Eqs. (10)–(13). To test the efficiency of the FLI, in Figure 2 we plot some curves showing the decrease of FLI with proper time τ for the same ordered and chaotic orbits as in the right of Figure 1. As is expected, there are two features : (*i*) the overgrowth of the geodesic deviation vector is much greater without post-stabilization of the constraint (15) than with (note the different vertical scales of the two panels) for both the regular orbit and the chaotic orbit; (*ii*) the geodesic deviation vector for the chaotic orbit G increases much faster than that of the ordered orbit F when τ reaches 10^5. In this time, the FLI of orbit F drops down to about -3 (i.e. $\|\boldsymbol{\xi}\| \approx 1000$), while the FLI of G decays exponentially and reaches -11, that is, eight orders of magnitude smaller. In Figure 1, both curves F and G evolve in a similar way up to proper time τ 3×10^4 and so do both curves (B) and (D). In Figure 2, after that point the FLI of orbit G decreases sharply and becomes -8 after proper time about 7×10^4, while the FLI of orbit F continues to follow the same power law of decrease. So, it is certain that orbit G is chaotic after integration time 7×10^4. However, the Lyapunov exponent of orbit G did not tend to the stable limit until integration time reaches 10^6 (see curve (D) in Fig. 1). In brief, it is cheaper to detect a significant feature using the FLI given by Eq. (25).

In the following, we use the FLI to explore the dynamics of the fixed points α (or β and γ), H and K of the Poincaré map (Figure 1). In particular, we are interested to know what effects on the dynamics are produced when we change some of the dynamical parameters.

Table 1 Classification of orbits for starting point α with $\mathcal{O} = 7.25 \times 10^{-7}$, $L = 3.8$ and different values of E

Interval of E	[0, 0.96]	[0.961, 0.9671]	0.9672	[0.9673, 0.9677]	0.9678	[0.9679, ∞)
type of orbit	no orbit	single torus	2 loops	3 islands	chaos	unstable

4.2 Effects of Distinct Parameters on Dynamical Features

As was stated in the above, the fixed points α (or β and γ), H and K each correspond to some closed periodic trajectories with resonant motion. Moreover, this implies the existence of more than three isolating integrals including Eqs. (5)–(7). Here we provide a rough illustration. In principle, the system (4) is equivalent to a superhamiltonian $\mathcal{H}(r, \theta, p_r, p_\theta)$ (Misner et al. 1970). Although the system is not globally integrable, for some special orbit one can find a canonical transformation from $(r, \theta, p_r, p_\theta)$ to the action-angle variables $(J_1, J_2, \theta_1, \theta_2)$ such that $\dot{J}_i = 0$ and $\dot{\theta}_i = \omega_i$ $(i = 1, 2)$. If the fundamental frequencies ω_i are incommensurate, the trajectory is quasi-periodic and not closed, and will densely cover the entire (θ_1, θ_2)-plane after an infinite time. However if the two frequencies are commensurate, then the motion is resonant and the orbit is closed and periodic [1]. As far as the chain of q islands is concerned, there is a mean motion resonance of the form $(p+q) : p$ with an integer p (Murray & Dermott 1999). Of course, the tori or chains close to these fixed points are viewed as forming the resonance regions. In spite of these facts it is very difficult to know p and resonance regions since it is not easy to express the system (4) in action-angle variables. Similarly, although we know that the resonance regions and locations of fixed points will change when we vary the dynamical parameters E, L and $\mathcal{O}$, we have some difficulties in finding them. So we want to understand what happens to the dynamical features at these invariant points of Figure 1.

Let E (=0.9675) and L (=3.8) be fixed but let $\mathcal{O}$ vary. The geodesic deviation equations with post-stabilization and the FLI are adopted, and numerical integration for each orbit does not stop till integration (proper) time reaches 10^5. Figure 3 shows the variation of the FLI with $\mathcal{O}$ for various orbits with the starting point α. It is clearly shown that all the FLI is greater than -5 for arbitrary $\mathcal{O}$ not exceeding 6.89×10^{-7}. This means the existence of many quasi-periodic orbits. Seen from the surface of section each of these quasi-periodic orbits is a single torus. When the octopolar parameter $\mathcal{O}$ increases from 6.89×10^{-7} to 6.97×10^{-7}, the FLI undergoes a sharp drop down to -17 or so, singnalling the onset of chaos. However, when $\mathcal{O}$ is inside the interval $[6.98 \times 10^{-7}$, $7.47 \times 10^{-7}]$, a chain of three loops appears. When $\mathcal{O}$ is close to the critical value 7.48×10^{-7}, then a set of chains involving multiple islands is produced. After this point, a new chaotic region appears. When $\mathcal{O} > 7.64 \times 10^{-7}$, the trajectory becomes unbounded. In short, the appearance of ordered or chaotic motion is very apparent from the variation of the FLI with $\mathcal{O}$. In other words, for a given E and L, we can successfully identify intervals of the octopolar parameter where the orbits are all regular or all chaotic. Here, an important point is that a chain with multiple loops is a necessary stage in the dynamical transition from ordered to chaotic. Of course, we also used the Poincaré surface of section as a check of the torus and island. We now fix $\mathcal{O} = 7.25 \times 10^{-7}$ and $L = 3.8$, and examine how the FLI varies with E. Table 1 lists some of the results obtained. Different types of orbits result from different values of E. An interesting point is that chaos occurs only when E is close to the value 0.9678. Of course, in a similar way we can study the case in which E and $\mathcal{O}$ are fixed and L varies.

The above operation was repeated for the starting point H in Figure 1, specifically, we examined the case when $\mathcal{O}$ changes but $E = 0.9675$ and $L = 3.8$ are fixed. As is shown in Figure 4 (top left panel), the FLI is larger than -6 in general, corresponding without doubt to regular orbits. As exceptional cases, chaos may occur near three points, labelled A, B and C, with $\mathcal{O}$ at 4.81×10^{-7}, 6.43×10^{-7} and 8.22×10^{-7}, respectively. More information is displayed by the orbits corresponding

[1] For a dynamical system with n degrees of freedom, the motion is resonant if there are more than n independent isolating integrals. The resonant orbit is not closed generally, but it is so when the system holds $2n - 1$ independent isolating integrals. For more information, see the references (Binney & Tremaine 1987; Carpintero & Aguilar 1998; Merritt 2001) where the orbits are shaped by their isolating integrals.

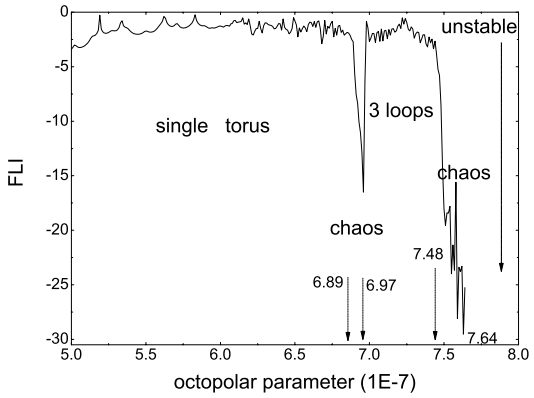

Fig. 3 Variation of the dynamical behavior with the octopolar parameter $\mathcal{O}$ for fixed parameters E (=0.9675), L (=3.8) and the starting point α.

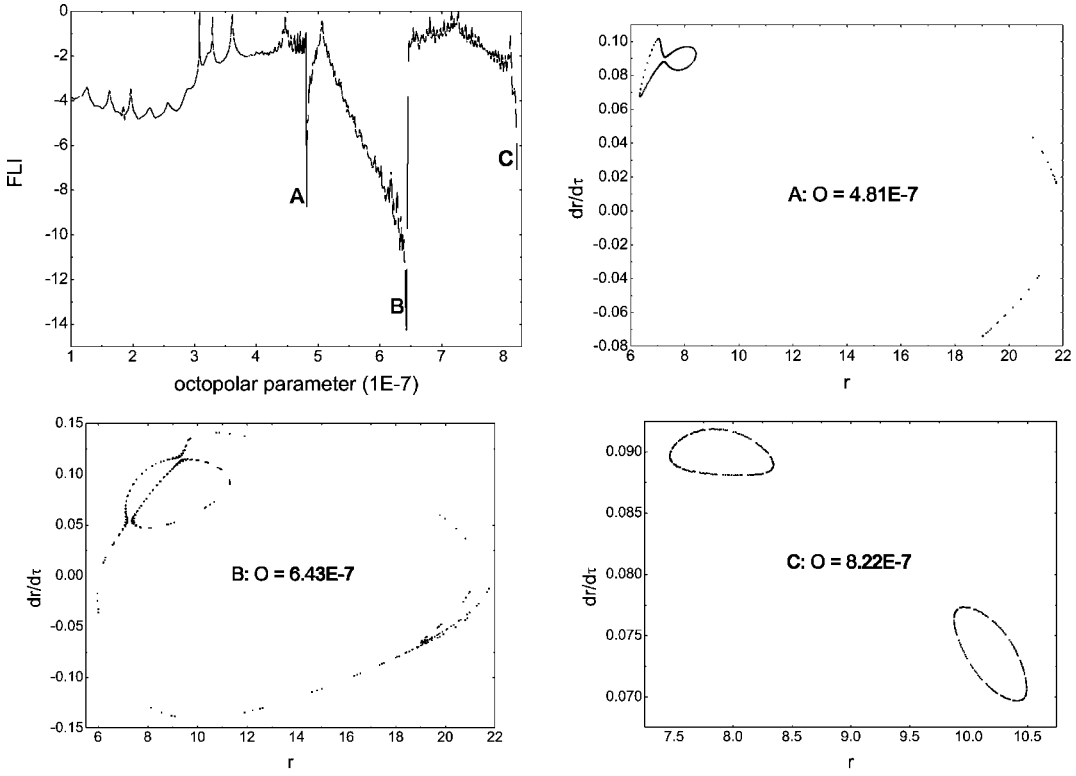

Fig. 4 Top left panel shows the variation of the FLI with the octopolar parameter $\mathcal{O}$ for the initial point H, with fixed E (=0.9675) and L (=3.8). The other three panels display the three orbits, A, B and C, on the Poincaré surface of section .

to the three cases in the Poincaré surface of section (the other three panels of Figure 4). Orbits A and B seem to give us the impression of regular motion. However, by convention, such "figure-of-8" orbits should mean chaotic motion in general. In fact, this is another characteristic of the stickiness phenomenon— the impression of ordered motion for long periods of time. Detection of this type of chaotic motion is difficult using the generic methods, but is easy with the FLI, showing again that the FLI is a very sensitive tool. As to orbit C, although the FLI drops down to about -7 it is still a regular orbit with two islands. Now, 8.22×10^{-7} is a critical value for $\mathcal{O}$ because once $\mathcal{O} \geq 8.23 \times 10^{-7}$, the particles will run to infinity. Indeed there exist more and more islands belonging to the same trajectory if $\mathcal{O}$ goes across the critical value and increases slightly. In this way, the onset of chaos is possible when $\mathcal{O}$ arrives at a certain value no greater than 8.23×10^{-7}. Perhaps this is a reason why the FLI falls obviously at the point C. Another possible interpretation is that the geodesic deviation vector grows rapidly when the particles are staying at the edge of some unstable region. We also examined the cases with the starting point K in Figure 1 as the octopolar parameter increases from zero. We found that the orbits remained bounded and ordered up to $\mathcal{O} = 1.6492 \times 10^{-6}$.

In sum, of the three fixed points α (or β and γ), H and K in Figure 1, point K is the most stable, while point α is the most unstable. It is extremely easy for chaos to arise in this kind of fixed point out of some perturbing factors.

5 SUMMARY

First, we presented the geodesic equations and the geodesic deviation equations for the Weyl spacetime in detail. We also gave some details on the implementation of post-stabilization in general relativity. The geodesic deviation vector with the post-stabilization of the constraint (15) can be used to calculate the Lyapunov exponents and the fast Lyapunov indicators with coordinate gauge invariance. Then, together with the Poincaré surface of section we made a more detailed study of the dynamics in a static axisymmetric spacetime comprising a Schwarzschild black hole plus a purely octopolar shell. Some of the results obtained in the present paper are summarized as follows.

(i) It is again found that the geodesic deviation vector without post-stabilization by the constraint (15) leads to overestimation of the Lyapunov exponents and fast Lyapunov indicators. Post-stabilization plays an important role in working out the problem.

(ii) An important point is that, by means of the fast Lyapunov indicator, we explored successfully the effects of different parameters on the dynamics at the fixed points α (or β and γ), H and K of the Poincaré map in Figure 1. Indeed, the fast Lyapunov indicator is a very fast and highly sensitive tool to discriminate between ordered and weak chaotic motions (the "stickiness" phenomenon). Using the fast Lyapunov indicator and the Poincaré surface of section, we can explore the different types of orbits as one of the three dynamical parameters E, L and $\mathcal{O}$ varies while keeping the other two fixed. In other words, we can easily identify intervals of the varying parameter that correspond to ordered or chaotic orbits. By specific examples, a chain with multiple islands is seen to be a necessary stage in the dynamical transition from ordered motion to chaotic motion.

We plan to use the fast Lyapunov indicator to describe the global phase space structure of the system and discuss the related resonance phenomena in detail in a future work.

Acknowledgements We would like to thank the anonymous referee and Professor Tian-Yi Huang for useful suggestions. This work is funded by the National Natural Science Foundation of China (Nos. 10303001, 10447112 and 10563001), Jiangsu Planned Projects for Postdoctoral Research Funds and the Science Foundation of Jiangxi Education Bureau.

APPENDIX

Christoffel Symbols and Their Corresponding Partial Derivatives

For the Weyl spacetime (4), all the non-vanishing Christoffel symbols are listed as follows:

$$
\begin{aligned}
&\Gamma^0_{01} = \Gamma^0_{10} = -\frac{1}{2}\Big(\frac{1}{r} - \frac{1}{r-2} - \frac{\partial P}{\partial r}\Big), && \Gamma^0_{02} = \Gamma^0_{20} = \frac{1}{2}\frac{\partial P}{\partial \theta},\\
&\Gamma^1_{00} = \frac{1}{2}\Big(1-\frac{2}{r}\Big)e^{2P-Q}\Big[\frac{2}{r^2} + \Big(1-\frac{2}{r}\Big)\frac{\partial P}{\partial r}\Big]; && \Gamma^1_{11} = -\Big[\frac{1}{r(r-2)} + \frac{1}{2}\Big(\frac{\partial P}{\partial r} - \frac{\partial Q}{\partial r}\Big)\Big],\\
&\Gamma^1_{12} = \Gamma^1_{21} = \frac{1}{2}\Big(\frac{\partial Q}{\partial \theta} - \frac{\partial P}{\partial \theta}\Big), && \Gamma^1_{22} = -(r-2)\Big[1 + \frac{r}{2}\Big(\frac{\partial Q}{\partial r} - \frac{\partial P}{\partial r}\Big)\Big],\\
&\Gamma^1_{33} = -\frac{1}{2}(r-2)e^{-Q}\sin^2\theta\cdot\Big(2 - r\frac{\partial P}{\partial r}\Big); && \Gamma^2_{00} = \frac{1}{2r^2}\Big(1-\frac{2}{r}\Big)e^{2P-Q}\frac{\partial P}{\partial \theta},\\
&\Gamma^2_{11} = -\frac{1}{2r(r-2)}\Big(\frac{\partial Q}{\partial \theta} - \frac{\partial P}{\partial \theta}\Big), && \Gamma^2_{12} = \Gamma^2_{12} = \frac{1}{2}\Big(\frac{2}{r} + \frac{\partial Q}{\partial r} - \frac{\partial P}{\partial r}\Big),\\
&\Gamma^2_{22} = \frac{1}{2}\Big(\frac{\partial Q}{\partial \theta} - \frac{\partial P}{\partial \theta}\Big), && \Gamma^2_{33} = -\frac{1}{2}e^{-Q}\sin\theta\Big(-\frac{\partial P}{\partial \theta}\sin\theta + 2\cos\theta\Big);\\
&\Gamma^3_{13} = \Gamma^3_{31} = -\frac{1}{2}\Big(\frac{\partial P}{\partial r} - \frac{2}{r}\Big), && \Gamma^3_{23} = \Gamma^3_{32} = -\frac{1}{2}\Big(\frac{\partial P}{\partial \theta} - 2\frac{\cos\theta}{\sin\theta}\Big).
\end{aligned}
$$

On the other hand, their partial derivatives are of the forms

$$
\begin{aligned}
\Gamma^1_{00,1} &= \Big[\frac{2}{r^2} + \Big(1-\frac{2}{r}\Big)\frac{\partial P}{\partial r}\Big]e^{2P-Q}\Big[\frac{1}{r^2} + \frac{1}{2}\Big(1-\frac{2}{r}\Big)\cdot\Big(2\frac{\partial P}{\partial r} - \frac{\partial Q}{\partial r}\Big)\Big]\\
&\quad + \frac{1}{2}\Big(1-\frac{2}{r}\Big)e^{2P-Q}\cdot\Big[-\frac{4}{r^3} + \Big(1-\frac{2}{r}\Big)\frac{\partial^2 P}{\partial r^2} + \frac{2}{r^2}\frac{\partial P}{\partial r}\Big],\\
\Gamma^1_{00,2} &= \frac{1}{2}\Big(1-\frac{2}{r}\Big)e^{2P-Q}\Big\{\Big(2\frac{\partial P}{\partial \theta} - \frac{\partial Q}{\partial \theta}\Big)\Big[\frac{2}{r^2} + \Big(1-\frac{2}{r}\Big)\cdot\frac{\partial P}{\partial r}\Big] + \Big(1-\frac{2}{r}\Big)\frac{\partial^2 P}{\partial r\partial\theta}\Big\};\\
\Gamma^1_{11,1} &= \frac{1}{r^2(r-2)} + \frac{1}{r(r-2)^2} - \frac{1}{2}\Big(\frac{\partial^2 P}{\partial r^2} - \frac{\partial^2 Q}{\partial r^2}\Big),\\
\Gamma^1_{11,2} &= -\frac{1}{2}\Big(\frac{\partial^2 P}{\partial r\partial\theta} - \frac{\partial^2 Q}{\partial r\partial\theta}\Big);\\
\Gamma^1_{12,1} &= \frac{1}{2}\Big(\frac{\partial^2 Q}{\partial r\partial\theta} - \frac{\partial^2 P}{\partial r\partial\theta}\Big),\\
\Gamma^1_{12,2} &= \frac{1}{2}\Big(\frac{\partial^2 Q}{\partial \theta^2} - \frac{\partial^2 P}{\partial \theta^2}\Big);\\
\Gamma^1_{22,1} &= -1 + (1-r)\Big(\frac{\partial Q}{\partial r} - \frac{\partial P}{\partial r}\Big) - \frac{r}{2}(r-2)\Big(\frac{\partial^2 Q}{\partial r^2} - \frac{\partial^2 P}{\partial r^2}\Big),\\
\Gamma^1_{22,2} &= -\frac{r}{2}(r-2)\Big(\frac{\partial^2 Q}{\partial r\partial\theta} - \frac{\partial^2 P}{\partial r\partial\theta}\Big);\\
\Gamma^1_{33,1} &= -\frac{1}{2}e^{-Q}\sin^2\theta\Big\{\Big(2 - r\frac{\partial P}{\partial r}\Big)\Big[1 - (r-2)\frac{\partial Q}{\partial r}] - (r-2)\Big(\frac{\partial P}{\partial r} + r\frac{\partial^2 P}{\partial r^2}\Big)\Big\},\\
\Gamma^1_{33,2} &= \frac{1}{2}(r-2)e^{-Q}\sin^2\theta\Big[\Big(2 - r\frac{\partial P}{\partial r}\Big)\cdot\Big(\frac{\partial Q}{\partial \theta} - 2\frac{\cos\theta}{\sin\theta}\Big) + r\frac{\partial^2 P}{\partial r\partial\theta}\Big];\\
\Gamma^2_{00,1} &= \frac{1}{r^2}e^{2P-Q}\Big\{\Big(1-\frac{2}{r}\Big)\Big[\Big(-\frac{1}{r} + \frac{\partial P}{\partial r} - \frac{1}{2}\frac{\partial Q}{\partial r}\Big)\cdot\frac{\partial P}{\partial \theta} + \frac{1}{2}\frac{\partial^2 P}{\partial r\partial\theta}\Big] + \frac{1}{r^2}\frac{\partial P}{\partial \theta}\Big\},\\
\Gamma^2_{00,2} &= \frac{1}{2r^2}e^{2P-Q}\Big(1-\frac{2}{r}\Big)\Big[\Big(2\frac{\partial P}{\partial \theta} - \frac{\partial Q}{\partial \theta}\Big)\frac{\partial P}{\partial \theta} + \frac{\partial^2 P}{\partial \theta^2}\Big];
\end{aligned}
$$

$$\Gamma^2_{11,1} = \frac{1}{2r(r-2)}\Big[\Big(\frac{1}{r}+\frac{1}{r-2}\Big)\Big(\frac{\partial Q}{\partial\theta}-\frac{\partial P}{\partial\theta}\Big)-\frac{\partial^2 Q}{\partial r\partial\theta}+\frac{\partial^2 P}{\partial r\partial\theta}\Big],$$

$$\Gamma^2_{11,2} = -\frac{1}{2r(r-2)}\Big(\frac{\partial^2 Q}{\partial\theta^2}-\frac{\partial^2 P}{\partial\theta^2}\Big);$$

$$\Gamma^2_{12,1} = \frac{1}{2}\Big(-\frac{2}{r^2}+\frac{\partial^2 Q}{\partial r^2}-\frac{\partial^2 P}{\partial r^2}\Big),$$

$$\Gamma^2_{12,2} = \frac{1}{2}\Big(\frac{\partial^2 Q}{\partial r\partial\theta}-\frac{\partial^2 P}{\partial r\partial\theta}\Big);$$

$$\Gamma^2_{22,1} = \frac{1}{2}\Big(\frac{\partial^2 Q}{\partial r\partial\theta}-\frac{\partial^2 P}{\partial r\partial\theta}\Big),$$

$$\Gamma^2_{22,2} = \frac{1}{2}\Big(\frac{\partial^2 Q}{\partial\theta^2}-\frac{\partial^2 P}{\partial\theta^2}\Big);$$

$$\Gamma^2_{33,1} = \frac{1}{2}e^{-Q}\sin^2\theta\Big[\frac{\partial Q}{\partial r}\Big(-\frac{\partial P}{\partial\theta}+2\frac{\cos\theta}{\sin\theta}\Big)+\frac{\partial^2 P}{\partial\theta\partial r}\Big],$$

$$\Gamma^2_{33,2} = \frac{1}{2}e^{-Q}\sin^2\theta\Big[\Big(\frac{\partial Q}{\partial\theta}-\frac{\cos\theta}{\sin\theta}\Big)\Big(-\frac{\partial P}{\partial\theta}+2\frac{\cos\theta}{\sin\theta}\Big)+\frac{\partial^2 P}{\partial\theta^2}+\frac{\partial P}{\partial\theta}\frac{\cos\theta}{\sin\theta}+2\Big].$$

References

Ascher U. M., 1997, Numerical Algorithms, 14, 1
Avdyushev V. A., 2003, Celest. Mech. Dyn. Astron., 87, 383
Baumgarte J., 1973, Celest. Mech., 5(4), 490
Binney J., Tremaine S., 1987, Galactic Dynamics, Princeton Univ. Press
Carpintero D. D., Aguilar L. A., 1998, MNRAS, 298, 1
Chin H., 1995, Ph.D. thesis, Institute of Applied Mathematics, University of British Columbia, Canada
Contopoulos G., Voglis N., Efthymiopoulos C., 1999, Celest. Mech. Dyn. Astron., 73, 1
Cornish N. J., 2001, Phys. Rev. D, 64, 084011
Cornish N. J., Levin J., 2002, Phys. Rev. Lett., 89, 179001
Froeschlé C., Lega E., 2000, Celest. Mech. Dyn. Astron., 78, 167
Froeschlé C., Lega E., Gonczi R., 1997, Celest. Mech. Dyn. Astron., 67, 41
Guéron E., Letelier P. S., 2001, A&A, 368, 716
Guéron E., Letelier P. S., 2002, A&A, Phys. Rev. E, 66, 6611
Hartl M. D., 2003, Phys. Rev. D, 67, 024005
Hartl M. D., 2003, Phys. Rev. D, 67, 104023
Hartl M. D., 2003, Ph.D. thesis, California Institute of Technology
Hénon M., Heiles C., 1964, AJ, 69, 73
Hobill D., Burd A., Coley A., eds., 1994, Deterministic Chaos in General Relativity, New York: Plenum Press
Imponente G., Montani G., 2001, Phys. Rev. D, 63, 103501
Karas V., Hure J.-M., Semerák O., 2004, Class. Quant. Grav., 21, 1
Levin J., 2000, Phys. Rev. Lett., 84, 3515
Merritt D., 2001, arXiv: astro-ph/0106082
Misner C. W., Thorne K. S., Wheeler J. A., 1970, GRAVITATION, W. H. Freeman and Compang San Francisco
Murray C. D., Dermott S. F., 1999, Solar System Dynamics, Cambridge University Press
Saa A., 2000, Phys. Lett. A, 269, 204
Saa A., Venegeroles R., 1999, Phys. Lett. A, 259, 201
Schnittman J. D., Rasio F. A., 2001, Phys. Rev. Lett., 87, 121101

Semerák O., Zellerin T., Žáček M., 1999, MNRAS, 308, 691
Semerák O., Zellerin T., Žáček M., 2001, MNRAS, 322, 207
Semerák O., Žáček M., 2000, PASJ, 52, 1067
Suzuki S., Maeda K. I., 1997, Phys. Rev. D, 55, 4848
Szydlowski M., 1997, Gen. Relativ. and Gravit., 29, 185
Tancredi G., Sánchez A., Roig F., 2001, AJ, 121, 1171
Vieira W. M., Letelier P. S., 1999, ApJ, 513, 383
Vieira W. M., Letelier P. S., 1997, Phys. Lett. A, 228, 22
Wang Y.-J., Huang Y.-B., 2001, ChJAA, 1(2), 125
Wu X., Huang T.-Y., 2003, Phys. Lett. A, 313, 77
Wu X., Huang T.-Y., 2005, Chin. Astron. Astrophys., 29, 81
Wu X., Huang T.-Y., Wan X.-S., et al., 2005, to be submitted to Phys. Rev. D
Wu X., Zhu J. F., He J. Z. et al., 2006, Comput. Phys. Commun., in press
Zhang F., 1996, Comput. Phys. Commun., 99, 53